energies

MDPI

Article

Tribo-Brake Characteristics between Brake Disc and Brake Shoe during Emergency Braking of Deep Coal Mine Hoist with the High Speed and Heavy Load

Dagang Wang *, Ruixin Wang, Tong Heng, Guozheng Xie and Dekun Zhang

School of Mechatronic Engineering, China University of Mining and Technology, Daxue Road #1, Xuzhou 221116, China; ruixinwang@cumt.edu.cn (R.W.); hengt@cumt.edu.cn (T.H.); TS19050056A31@cumt.edu.cn (G.X.); dkzhang@cumt.edu.cn (D.Z.)

* Correspondence: wangdg@cumt.edu.cn; Tel.: +86-516-83591916

Received: 16 August 2020; Accepted: 25 September 2020; Published: 30 September 2020

Abstract: The friction wear and thermal fatigue cracking of the brake shoe and friction-induced self-excited vibration (frictional flutter) of the disc brake can easily occur during emergency braking of a deep coal mine hoist with at high speed and with a heavy load. Therefore, tribo-brake characteristics between the brake disc and brake shoe during emergency braking of a deep coal mine hoist are investigated in the present study. Scaled parameters of the disc brake of a deep coal mine hoist are determined by employing the similarity principle. Friction tests between friction disc and brake shoe are carried out to obtain the coefficient of friction in the case of high speed and large specific pressure between the friction disc and brake shoe. Coupled thermo-mechanical finite element analyses of the brake disc and brake shoe are established to investigate temperature and stress fields of the brake disc and brake shoe during emergency braking, which is validated by the engineering failure case. Effects of braking parameters on flutter characteristics between the brake disc and brake shoe are explored by employing a double-degrees-of-freedom vibration mechanism model. The results show that the maximum temperature, equivalent Von Mises stress and contact pressure are all located at the average friction radii of contact surfaces of the brake disc and brake shoe during emergency braking. The cage crashing accident in the case of high speed and heavy load in a typical coal mine shows crack marks and discontinuous burn marks at central locations of brake shoe and brake disc surfaces, respectively, which indicates frictional flutter characteristics between brake disc and brake shoe. During emergency braking, flutter time duration decreases with increasing initial braking speed and damping parameter; the flutter amplitude and frequency of the disc brake increases with increasing normal braking load and stiffness, respectively.

Keywords: deep coal mine; emergency braking; tribo-brake; high speed; heavy load

1. Introduction

The multi-rope friction hoisting system in coal mine (See Figure 1 in [1]) is used to lift and lower the coal, gangue, equipment and personnel. As is known, 53% of China's coal resources are buried below the kilometer stratum. The deep coal mine hoist exhibits the high hoisting speed up to 20 m/s and heavy terminal load up to 100 tons. The disc brake, with brake shoes symmetrically located at both sides of the brake disc (See Figure 1 in [1]), provides enough brake torque and preset brake deceleration in order to brake the friction hoist safely and reliably. During emergency braking in the deep coal mine with high speed and high specific pressure, the friction and friction-induced heat between contact surfaces of brake disc and brake shoe present the stress and temperature fields, respectively, the interaction of which results in coupled thermo-mechanical properties at contacting

surfaces. Meanwhile, the friction-induced self-excited vibration (frictional flutter) of brake disc and brake shoe easily occur. Therefore, it is of great significance to explore tribo-brake characteristics between brake disc and brake shoe (coupled thermo-mechanical and flutter characteristics between brake disc and brake shoe) during emergency braking of a deep coal mine hoist under high speed and heavy load conditions in order to assure the brake safety and brake reliability and thereby to avoid significant malignant accidents of wellbore destruction and personnel death or injury.

In recent years, many scholars have carried out studies on thermal stress behaviors of disc brake during emergency braking at low speed and at a specific pressure in a shallow coal mine. Wang et al. [1] studied dynamic brake characteristics (brake torque, thermo-mechanical coupled behavior) of disc brake during emergency braking of the kilometer deep coal mine hoist. Zhu et al. [2] analytically studied the temperature field of the brake shoe during emergency braking. Peng et al. [3] explored temperature fields of the brake disc and brake shoe during braking and found better thermal conductivity and a lower temperature gradient of the brake disc. Bao et al. [4] studied the tribological properties of the brake shoe at different brake pressures and found that the wear rate and average surface temperature both increase with increasing brake pressure. Yevtushenko et al. [5,6] analyzed the effect of surface structure of brake material on the temperature field of friction surface, and explored the mutual influence of the sliding velocity and temperature on frictional heating of the thermally nonlinear disc brake. Zhou et al. [7] studied mechanisms of the heat generation and transmission during braking and analyzed temperature distributions of the brake disc at different initial braking speeds. Furthermore, many researchers have analyzed coupled thermo-mechanical properties of the disc brake of passenger car during emergency braking [8–11]. However, considering flutter characteristics of the brake system, lots of researches have been focused on the fields of aviation, high-speed rail and passenger car. Li et al. [12] employed the single-degree-of-freedom model to study effects of damping ratio and friction parameter on the critical speed of flutter motion. Eriksson et al. [13] studied the flutter characteristics of braking device and found friction mainly caused the flutter and noise. Manish et al. [14] analyzed effects of system stiffness, damping factor and coefficient of friction on the flutter characteristics of a brake system. However, for the case of emergency braking of a disc brake with high initial braking speed and large specific pressure in a deep coal mine, coupled thermo-mechanical characteristics and flutter characteristics between brake disc and brake shoe have not been reported yet.

Therefore, the research objective of this paper is to explore tribo-brake characteristics between brake disc and brake shoe in the deep coal mine at high speed and with a heavy load. Section 2 presents the thermo-mechanical finite element model of brake disc and brake shoe. Coupled thermo-mechanical simulation results of brake disc and brake shoe are presented in Section 3. Frictional flutter characteristics between brake disc and brake shoe are investigated in Section 4. Section 5 presents the conclusions of this study.

2. Thermo-Mechanical Finite Element Model of Brake Disc and Brake Shoe

2.1. Calculation of Prototype Model Parameters of the Disc Brake of Deep Coal Mine Hoist

During emergency braking, the tribo-brake between brake shoes and brake disc causes the conversion of kinetic energy of hoisting system into the frictional work. The mass of various components of hoisting system is transferred to the drum for simplicity. Therefore, the kinetic energy of various components of the hoisting system is equal to the kinetic energy of the total equivalent mass of the drum as shown in Equation (1). The kinetic energy of the drum after transformation is given by Equation (2) according to the moment of inertia. The equal frictional work consumed during emergency braking of hoisting system before and after transformations can be described as Equation (3). According to Equations (1)–(3), Equation (4) can be obtained [15].

$$W_f = \frac{1}{2} M_f {V_f}^2 = \frac{1}{2} M_f (\omega_f R_f)^2 \quad (1)$$

$$W_w = \frac{1}{2} J_w {\omega_w}^2 \tag{2}$$

$$\frac{1}{2} M_f (\omega_f R_f)^2 = \frac{1}{2} J_w {\omega_w}^2 \tag{3}$$

$$J_w = M_f {R_f}^2 \tag{4}$$

where M_f is the total equivalent mass of hoisting system, R_f is the radius of brake disc, V_f is the hoisting speed, ω_f is the angular velocity of drum before transformation, J_W and ω_W are moment of inertia and angular velocity of drum after transformation, respectively. In Equations (1)–(4), the effects of air resistance and lateral force are ignored.

According to parameters in Table 1, the total equivalent mass of hoisting system is 172.8 tons. In order to investigate emergency braking characteristics of a disc brake during hoisting at a high speed and with a heavy load, we assume the lifting height of 1000 m, maximum hoisting speed of 20 m/s, emergency braking deceleration of 1.6 m/s^2 and brake-specific pressure of 1.6–2.0 MPa. Therefore, the total moment of inertia of hoisting system and rotational speed of hoist drum can be described as Equations (5) and (6), respectively.

$$J_1 = M_f {R_f}^2 = 172800 \times 2.5^2 = 1.08 \times 10^6 \, \mathrm{kg \cdot m^2} \tag{5}$$

$$n_1 = \frac{V_w}{2\pi R_w} = \frac{20}{2\pi \times 2.5} = 76.4 \, \mathrm{r/min} \tag{6}$$

Table 1. JKMD-5 × 4(III)-type floor multi-rope friction hoisting system in Guqiao coal mine in China.

Equivalent Mass (tons)				Maximum Static Tension Difference of Hoist (tons)	Diameter of Brake Disc (m)	Pairs of Brake Shoe	Area of a Brake Shoe (m^2)	Maximum Brake Pressure (kN)
Hoist	Motor	Effective Load	Sheave					
32.2	9.52	60	39.4	91.68	5	12	0.0494	160–200

2.2. Determination of Scaled Parameters of Disc Brake of the Deep Coal Mine Hoist

The main physical parameters in the prototype and scaled models during emergency braking can be found in Table 2. The similarity principle is employed to obtain similarity constants of main physical parameters in both models.

Table 2. Main physical parameters in the prototype and scaled models during emergency braking.

	Prototype Model	Scaled Model	Similarity Coefficient
Radius of brake disc	r_1 (m)	r_2 (m)	$K_r = r_2/r_1$
Spindle speed	n_1 (r/min)	n_2 (r/min)	$K_n = n_2/n_1$
Moment of inertia	J_1 (kg·m^2)	J_2 (kg·m^2)	$K_J = J_2/J_1$
Friction radius	R_1 (m)	R_2 (m)	$K_R = R_2/R_1$
Brake torque	M_1 (N·m)	M_2 (N·m)	$K_M = M_2/M_1$
Number of friction surface	C_1	C_2	$K_C = C_2/C_1$
Friction surface area	S_1 (m^2)	S_2 (m^2)	$K_S = S_2/S_1$
Friction work per unit area	E_1 (J)	E_2 (J)	$K_E = E_2/E_1$
Angular deceleration during braking	α_1 (m/s^2)	α_2 (m/s^2)	$K_a = \alpha_2/\alpha_1$

(1) Friction radius of brake disc

The similarity coefficient of spindle speed is written as Equation (7) [16]. Attributed to the same speed at the friction radius in prototype and scale models, the similarity coefficient K_V is equal to 1 according to $K_V = K_R K_n$ and thus $K_R = 1/K_n = 0.06$. According to the similarity coefficient of friction radius $K_R = R_2/R_1$ and $R_1 = 2.5$ m, friction radius in the scale model R_2 is equal to 0.15 m.

$$K_n = \frac{n_2}{n_1} = \frac{1280}{76.4} = 16.75 \tag{7}$$

where the spindle speed n_2 in the scaled model is assumed to be 1280 r/min and spindle speed n_1 in the prototype model is equal to 76.4 r/min as shown in Section 2.1.

(2) Geometric dimension of brake shoe

The brake shoe presents the same material, a similar geometric shape and a proportional change of geometric dimension in scaled and prototype models. The length, width and thickness of the brake shoe in the scaled model are 50 mm, 30 mm and 10 mm, respectively. In the prototype model, frictional area of the brake shoe is 49,400 mm^2. Therefore, the similarity coefficient of friction surface area is written as $K_S = S_2/S_1 = 0.03$.

(3) Moment of inertia

In the prototype model, there are 24 friction surfaces between brake disc and brake shoe, while there is only one friction surface in the scale model. According to the similarity coefficient of number of friction surface $K_C = C_2/C_1 = 1/24$ and the similarity principle, the similarity coefficient of moment of inertia can be described as $K_J = K_R^2 \cdot K_C K_S = J_2/J_1$. Therefore, the moment of inertia of the brake disc in the scaled model is written as [16]

$$J_2 = J_1 \cdot K_R^2 K_C K_S = 4.86 \text{ kg} \cdot \text{m}^2 \tag{8}$$

(4) Specific pressure

Scaled and prototype models have the same specific pressure, i.e., $P_1 = P_2 = 1.6$ MPa. The similarity coefficient of specific pressure K_P is described as Equation (9) [16], which indicates $K_p = K_F/K_S = 1$ and thereby $K_F = K_S$. According Equation (8), we can obtain $F_2 = F_1 K_S = P_1 S_1 K_S = 2400$ N.

$$K_P = \frac{P_2}{P_1} = \frac{F_2}{F_1}\frac{S_1}{S_2} = 1 \tag{9}$$

2.3. Material Parameters

According to calculated results in Section 2.1, the brake disc of Q345 alloy steel has inner and outer diameters of 260 mm and 340 mm, respectively, a thickness of 10 mm and an average friction diameter of 150 mm. The WSM-3 non-asbestos resin-based brake shoe is mainly composed of phenolic resin, NBR, vermiculite powder, conductive carbon black, alumina ceramic fiber, graphite, sepiolite, wollastonite, barium sulfate and diatomite. The WSM-3 brake shoe has inner and outer diameters of 270 mm and 330 mm, respectively, a thickness of 10 mm, an average friction diameter of 150 mm and the arc angle of 20°. Material parameters of brake disc and brake shoe can be found in Table 3.

Table 3. Material parameters of brake disc and brake shoe [17].

	Density (kg/m^3)	Young's Modulus (Pa)	Poisson's Ratio	Thermal Expansion Coefficient (10^{-5}/K)	Thermal Conductivity (W/(m·K))	Specific Heat Capacity (J/(kg·K))
Brake shoe	2250	2.2×10^9	0.25	3	1.4	2550
Brake disc	7850	2.09×10^{11}	0.3	1.2	58	460

2.4. Determination of Finite Element Model Parameters

(1) Coefficient of friction

The JF151E brake shoe friction test rig in CITIC Heavy Industries CO., LTD (Figure 1) is employed to carry out friction tests between friction disc and brake shoe. The length, width and thickness of

brake shoe specimen are 20 mm, 30 mm and 8 mm, respectively. In the test rig, the motor rotates the friction disc through the belt transmission and the motor speed is controlled by the frequency converter. The weight is amplified by the lever to apply the contact load between friction disc and brake shoe, and the contact pressure ranges from 1.6 to 2.0 MPa. The contact load can be measured by the tension-compression type transducer. Heating pipes and cooling devices are installed under the friction disc in order to keep the constant temperature during the test. The thermocouple is located near the contact surface of friction disc to measure the temperature. The industrial control computer is employed to collect the temperature and friction force. Therefore, the coefficient of friction can be calculated by the friction force divided by the contact load.

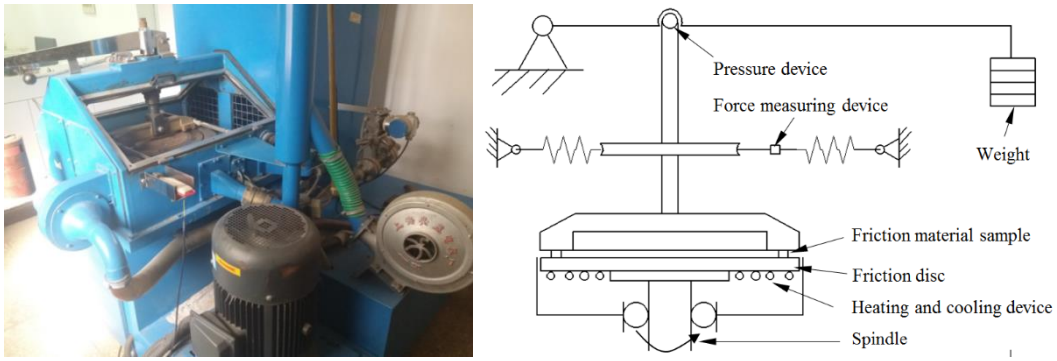

Figure 1. JF151E-type friction test apparatus of the brake shoe and its principle diagram.

Generally, the temperature of brake disc and brake shoe during emergency braking is less than 100 °C; the maximum temperature of friction surfaces ranges from 60 to 100 °C, and the coefficient of friction decreases with increasing temperature. In order to ensure the braking safety and reliability in the actual emergency braking conditions, the coefficient of friction between brake shoe and friction disc at 100 °C is chosen. Figure 2 shows that the coefficient of friction increases at first and then stabilizes with increasing rotation cycles in each contact pressure case. An increase in contact pressure causes an overall decrease at ~2000 cycles; after 2000 cycles, the coefficient of friction decreases at first and then increases. The average coefficient of friction between contacting interfaces in cases with five contact pressures is 0.423. However, previous research indicates that the coefficient of friction between brake shoe and friction disc is smaller than 0.4 [17]. Therefore, the coefficient of friction between brake shoe and friction disc is set as 0.4 for simplicity in the present study.

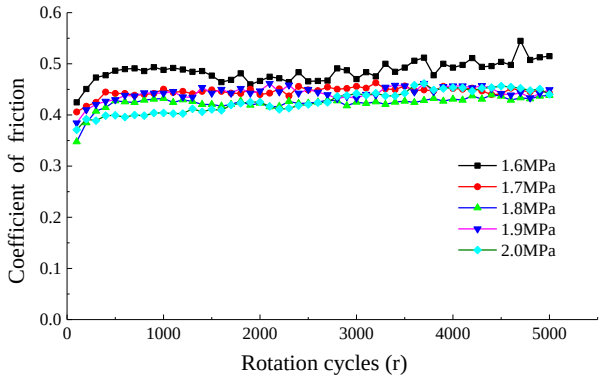

Figure 2. Evolutions of coefficients of friction between friction disc and brake shoe at different contact pressures.

(2) Angular velocity during braking

It is known that the rotational linear velocity and angular velocity of friction disc are 20 m/s and 133.33 rad/s, respectively. The braking moment during emergency braking is written as

$M_2 = \mu F_2 R_2 = J_2 \alpha_2$. Therefore, angular deceleration of brake disc during braking is given by $\alpha_2 = \mu F_2 R_2 / J_2$, and thereby $\alpha_2 = 29.6$ rad/s^2 according to parameters F_2, R_2 and J_2 in Section 2.2 and coefficient of friction. The angular velocity of brake disc during emergency braking is described as $\omega = 133.33 - 29.6t$.

(3) Convective heat transfer coefficient

The convective heat transfer coefficient between brake disc and air is given by [18]

$$h = \begin{cases} 0.7\left(\frac{\lambda_a}{d_a}\right)R_e^{0.55} & R_e \le 2.4 \times 10^5 \\ 0.04\left(\frac{\lambda_a}{d_a}\right)R_e^{0.8} & R_e \ge 2.4 \times 10^5 \end{cases} \quad (10)$$

where R_e, Reynolds number, is written by $R_e = \frac{v_a \rho_a d_a}{3.6\mu_a}$. In the equation, v_a is the speed of brake disc, i.e., $v_a = \omega \cdot R_f$, ρ_a is the air density, d_a is the outer diameter of brake disc, μ_a is the air viscosity and λ_a is the heat transfer coefficient of air. Assuming the air temperature of 20 °C, we can obtain $\rho_a = 1.164$ kg/m^3, $\mu_a = 18.24 \times 10^{-6}$ Pa·s and $\lambda_a = 2.524 \times 10^{-2}$ W/(m·K). Substitutions of those parameters into Reynolds number equation and Equation (10) deduce $R_e = 5318$ and $h = 6.595$ W/(m^2·K) at the angular velocity of 1 rad/s as well as $R_e = 709{,}046$ and $h = 161.276$ W/(m^2·K) at the angular velocity of 133.33 rad/s.

2.5. Coupled Thermo-Mechanical Finite Element Model of Brake Disc And Brake Shoe

The three-dimensional contact model of brake disc and brake shoe established by Creo is imported into the finite element software ABAQUS to construct the finite element model. The coupled thermo-mechanical module in ABAQUS is employed to analyze coupled thermo-mechanical behaviors of brake disc and brake shoe during emergency braking. During the analysis, materials of brake disc and brake shoe are assumed to be homogeneous and isotropic. The wear at contacting surfaces is ignored, and heat conduction and convection are mainly focused on. The convective heat transfer coefficient as indicated above is applied to contacting surfaces. The initial ambient temperature is set as 20 °C. It is assumed that 90% kinetic energy due to tribo-brake is converted into the heat energy. The reference point is employed to couple nodes of brake disc surface using the continuum coupling method. The uniform pressure is applied to the outer surface of brake shoe. The rotational speed and direction of brake disc are defined through the reference point. The brake shoe is allowed to move along the normal direction of contacting brake disc and brake shoe. Other degrees of freedom of brake disc and brake shoe are fixed. The C3D8RT thermo-mechanical coupling unit in ABAQUS is employed to mesh the brake disc and brake shoe. The brake disc and brake shoe have 2880 and 120 elements, respectively, and 4050 and 210 nodes, respectively (Figure 3). Fine meshes are employed near contact surfaces of brake disc and brake shoe attributed to large change rates of temperature and stress near contact surfaces. The loading procedure can be found in Table 3. The fourth analysis step corresponds to the emergency braking. During emergency braking, $\omega = 133.33 - 29.6t$. In the equation, t is braking time and ω denotes the rotational speed of brake disc. Table 4 shows the loading procedure of the finite element analysis.

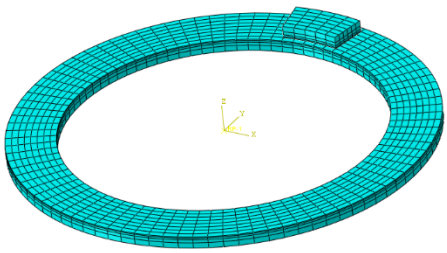

Figure 3. Three-dimensional contact finite element model of brake disc and brake shoe.

Table 4. Loading procedure of the finite element analysis.

Analysis Step	Contact Pressure (Pa)	Rotational Speed (rad/s)	Time (s)
1	10	0	0.001
2	1.6×10^6	1	0.001
3	1.6×10^6	133.33	0.001
4	1.6×10^6	ω	4.5

3. Coupled Thermo-Mechanical Simulation Results of Brake Disc and Brake Shoe

3.1. Temperature and Stress Distributions of Brake Disc and Brake Shoe During Emergency Braking

3.1.1. Temperature Distribution

Figure 4 shows that temperature of brake disc and brake shoe both presents large values at the average friction radius, and decreases towards both sides along the radial direction, which is attributed to the high contact pressure and poor thermal convection effect at contact regions of brake disc and brake shoe. The temperature field of brake shoe surface decreases from the outlet to the inlet attributed to the gradual superimposition of friction heat from the inlet to the outlet. The temperature field of brake disc decreases along the rotational direction attributed to the heat conduction and convective heat transfer. The brake disc and brake shoe both exhibit the maximum temperature fields at 2.41 s during emergency braking attributed to the balance among friction heat, heat conduction loss and convective heat transfer.

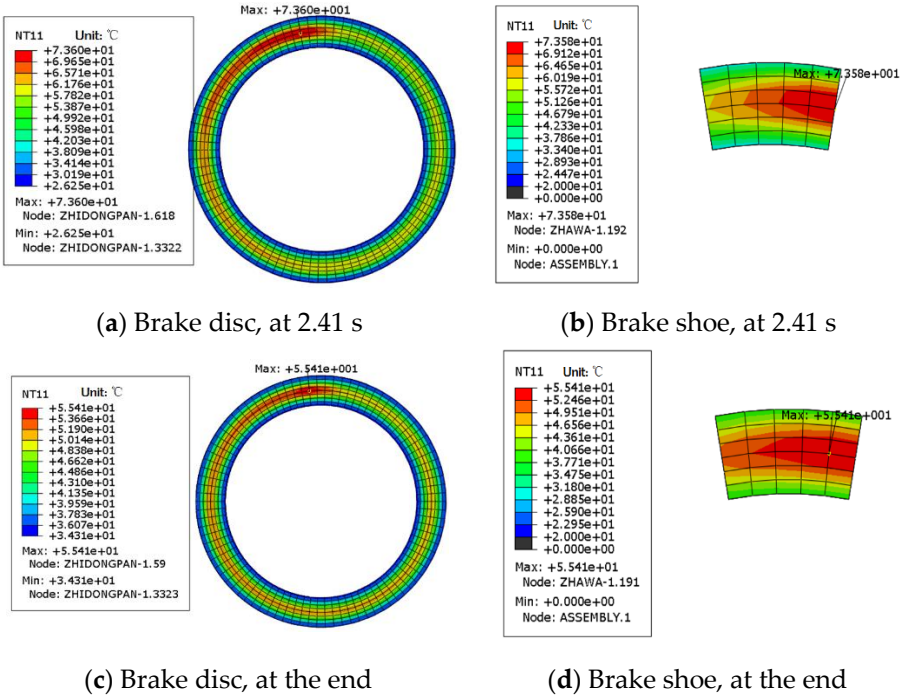

(**a**) Brake disc, at 2.41 s (**b**) Brake shoe, at 2.41 s

(**c**) Brake disc, at the end (**d**) Brake shoe, at the end

Figure 4. Temperature distributions at contact surfaces of brake disc and brake shoe during emergency braking (counterclockwise rotation of brake disc).

3.1.2. Equivalent Stress Distribution

Figure 5a,b shows ring-shaped high equivalent Von Mises stress distribution at the average friction radius of brake disc surface and an overall decrease in the equivalent Von Mises stress from the inlet to the outlet of brake shoe surface. The high equivalent stress at the inlet of brake shoe surface is caused by the stress concentration due to shape edge effect. Figure 5a,c,e shows an increase at first and then a decrease in the equivalent stress with increasing braking time at the brake disc surface,

while Figure 5b,d,f exhibits an increase in the equivalent stress with increasing braking time at the brake shoe surface. Brake disc and brake shoe surfaces exhibit the maximum equivalent stresses of 80.78 MPa and 1.35 MPa, respectively, at 1.32 s and at the end during emergency braking.

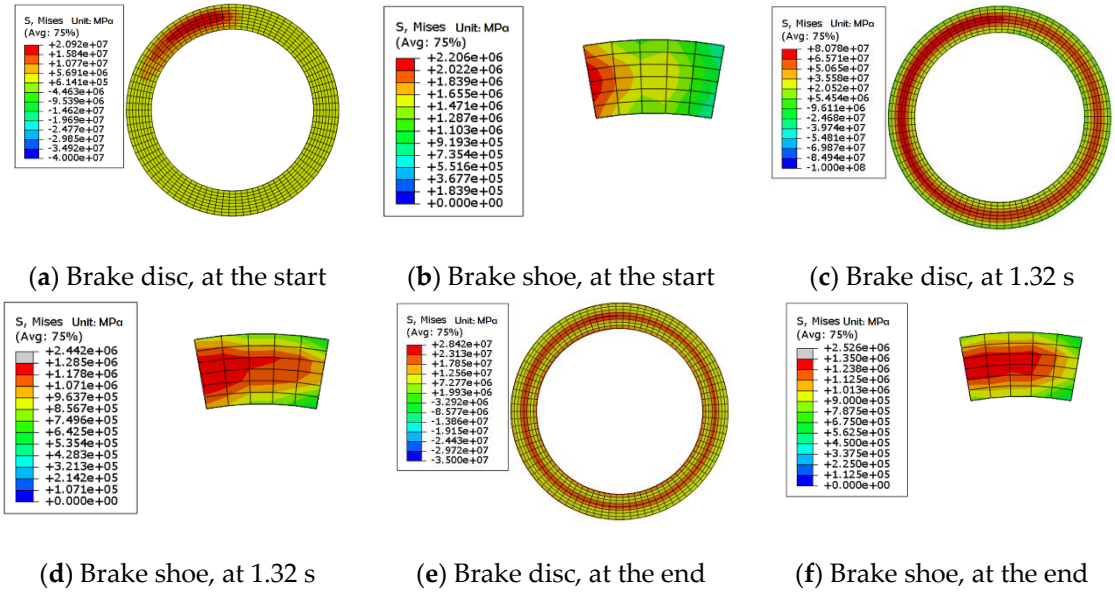

(**a**) Brake disc, at the start (**b**) Brake shoe, at the start (**c**) Brake disc, at 1.32 s

(**d**) Brake shoe, at 1.32 s (**e**) Brake disc, at the end (**f**) Brake shoe, at the end

Figure 5. Equivalent stress distributions at contact surfaces of brake disc and brake shoe during emergency braking.

3.2. Evolutions of Temperature And Stress Distributions of Brake Disc And Brake Shoe during Emergency Braking

In order to quantitatively demonstrate three-dimensional temperature and stress distributions of brake disc and brake shoe during emergency braking, we choose nodes A-G and A′-G′ along the radial directions of brake disc and shoe surfaces, respectively, as shown in Figures 6a and 7a, and nodes 1–5 and 1′–5′ along the axial directions at the average friction radii of brake disc and shoe surfaces, respectively, as shown in Figures 6b and 7b.

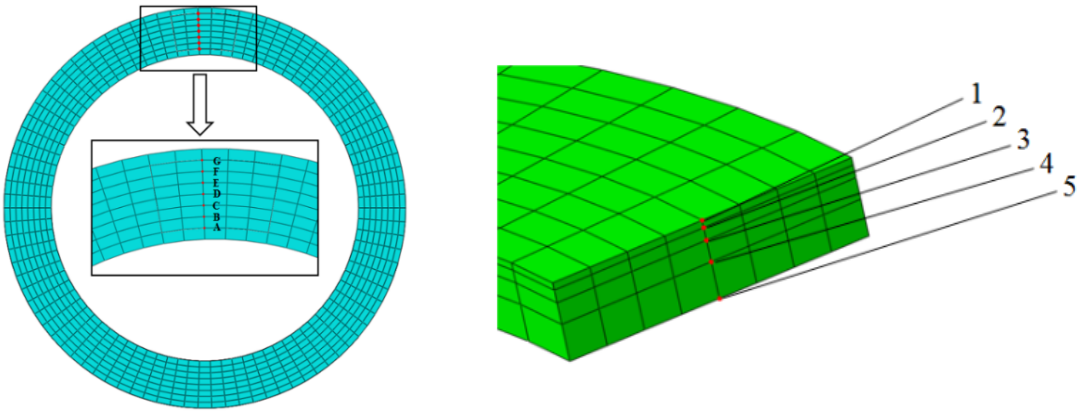

Figure 6. Distributions of nodes along different paths of brake disc.

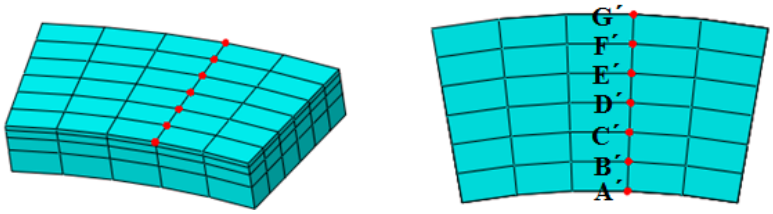

(**a**) Along the radial direction

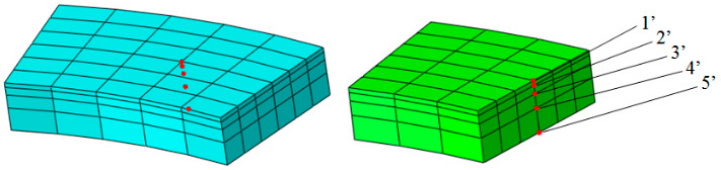

(**b**) Along the axial direction at the average friction radius

Figure 7. Distributions of nodes along the different paths of brake shoe.

3.2.1. Temperature Distribution

Figure 8a shows sawtooth fluctuations of temperature evolution curves of various nodes along the radial direction of brake disc surface attributed to alternating thermal shock caused by friction and convective heat transfer [19]. An increase in time causes the more obvious sawtooth fluctuation of temperature evolution curve and the gradual increase in the time interval between adjacent sawteeth. At the start of emergency braking, the small sawtooth fluctuation is attributed to the larger friction heat generation than the heat dissipation caused by the high rotational speed of brake disc. At the later stage, a decrease in the rotational speed of brake disc induces a rise in temperature and an increase in heat dissipation. The strong alternating effect of heat generation and dissipation causes the obvious sawtooth fluctuation. The temperature evolution curve of each node at the brake disc surface exhibits the maximum value at a certain time during emergency braking attributed to the equilibrium state between the heat generation and heat dissipation due to heat transfer and conduction. Comparisons of temperature evolution curves at different friction radii indicate that an increase in friction radius causes the overall increase at first and then a decrease in the node temperature. The highest temperature occurs at the average friction radius, i.e., node D, which indicates the location at the average friction radius is less affected by heat convection and conduction. Equidistant points at both sides of the node at the average friction radius present approximately the same change law of temperature evolution curve. The temperature decreases along the radial direction from node D towards both sides, which indicates the location at the average friction radius (node D) is less affected by the heat convection and conduction and coincides well with results in Section 3.1.

Figure 8b shows the smooth temperature evolution curve without the obvious sawtooth in all cases. That is because the heat dissipation attributed to convective heat transfer between brake shoe and area is smaller as compared to that between brake shoe and brake disc. During emergency braking, each temperature curve presents an increase at first and then a decrease with increasing brake time. At the start of emergency braking, the large rotational speed of brake disc causes lots of frictional heat which accumulates quickly at the short time, which induces the rapid increase in the temperature of brake shoe surface. The temperature rise is larger at the location closer to the average friction radius. At the intermediate stage, the rotational speed of the brake disc decreases and the frictional heat generated decreases. The brake shoe presents a heat balance between the heat generation and heat dissipation due to heat conduction and convective heat transfer. Therefore, the temperature of each node at the brake shoe surface increases slowly at first and then reaches a maximum value. At the later stage, the low rotational speed of the brake disc causes heat generation smaller than the heat dissipation due to heat conduction and convective heat transfer, which reveals an overall decrease

in the temperature of brake shoe surface. Comparisons of temperature curves of various nodes at different friction radii indicate that an increase in friction radius induces an overall increase at first and then a decrease in the node temperature, which reveals the location at the average friction radius less affected by the convective heat transfer and heat conduction.

Figure 8c shows a larger temperature gradient along the axial direction at the average friction radius of brake disc during emergency braking. A larger distance to the contact surface exhibits the lower temperature. Node 1 at the contact surface of brake disc presents the sawtooth shaped temperature evolution curve attributed to the thermal shock and convective heat dissipation. The temperature evolution curve of node 2 presents the sawtooth fluctuation with a small amplitude mainly attributed to the heat conduction of sawtooth-shaped temperature variation at the brake disc surface and the decreased role of convection heat dissipation. Nodes 3, 4 and 5 are situated away from the friction surface of brake disc in turn. An increase in axial distance to the contact surface causes a decrease in the conduction of frictional heat. Therefore, the temperature presents the overall decrease along the axially outward direction from the contact surface. Attributed to small effects of frictional heat shock and convective heat dissipation, temperature evolution curves of nodes 3, 4 and 5 all present smooth upward variation trends. As the distance to contact surface increases, the location of highest temperature moves towards the end of emergency braking, which reveals the hysteresis of heat conduction.

Figure 8d shows that the temperature evolution curve of brake shoe presents the large gradient along the axial direction at the average friction radius of brake shoe during emergency braking. An increase in the distance to the contact surface of brake shoe along the axial direction induces the overall decrease in the node temperature. During emergency braking, the hysteresis of heat conduction induces the gradual increase in node temperature evolution curve in cases of nodes 2′ and 3′. At nodes 4′ and 5′, the node temperature almost presents unobvious change attributed to the low coefficient of heat conduction and poor thermal conductivity of the brake shoe.

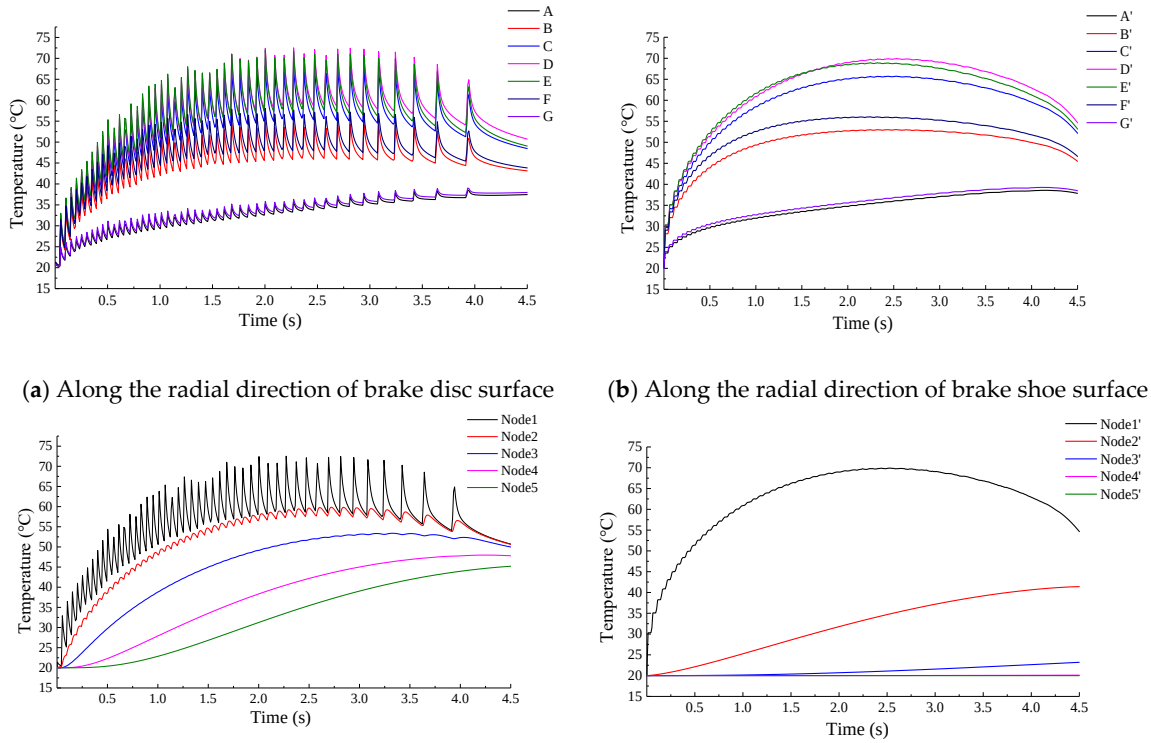

(**a**) Along the radial direction of brake disc surface

(**b**) Along the radial direction of brake shoe surface

(**c**) Along the axial direction at the average friction radius of brake disc

(**d**) Along the axial direction at the average friction radius of brake shoe

Figure 8. Temperature distributions along radial and axial paths of brake disc and brake shoe during emergency braking.

3.2.2. Equivalent Von Mises Stress Distribution

Figure 9a shows an overall increase at first and then a decrease in the evolution of equivalent Von Mises stress of each node at the brake disc surface with the sawtooth fluctuation. The sawtooth fluctuation is obvious and is close to the average friction radius. Along the radial direction of the brake disc surface, an increase in friction radius induces the overall increase at first and then a decrease in the equivalent stress. The equivalent stress reaches the maximum value at the average friction radius attributed to the larger temperature rise and easier production of thermal stress. Figure 9b shows that the equivalent stress evolution curve of the node along the axial direction of locations at the average friction radius of brake disc surface presents the overall increase at first and then a decrease. The equivalent stress evolution at the location closer to brake disc surface presents more obvious sawtooth fluctuation. Along the axial direction, the temperature change between adjacent nodes increases at first and then decreases, which induces the increase at first and then a decrease in the equivalent stress. An increase in the distance to the contact surface, the equivalent stress presents the overall decrease trend.

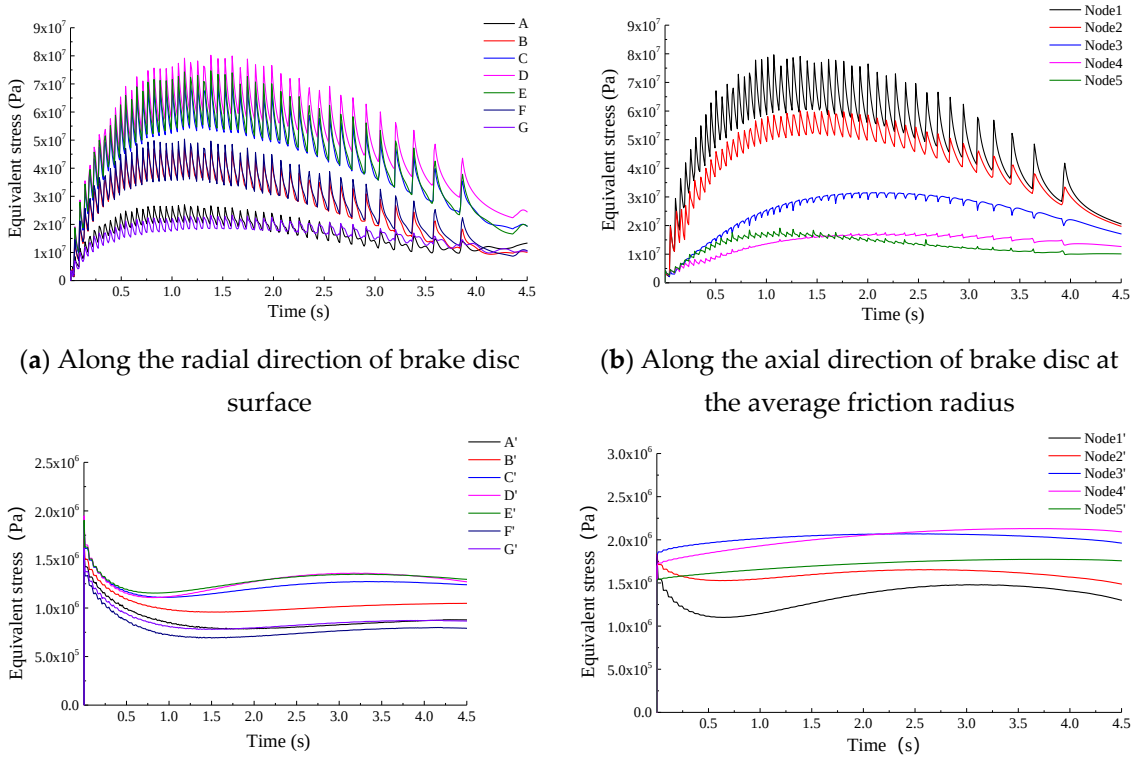

(**a**) Along the radial direction of brake disc surface

(**b**) Along the axial direction of brake disc at the average friction radius

(**c**) Along the radial direction of brake shoe surface

(**d**) Along the axial direction of brake shoe at the average friction radius

Figure 9. Equivalent Von Mises stress distributions of brake disc and brake shoe along radial and axial paths during emergency braking.

Figure 9c shows that the equivalent stress evolution curve of each node at the brake shoe surface presents an overall decrease at first, then a decrease and the final stabilization. Meanwhile, the equivalent stress reaches the maximum value at the average friction radius. Figure 9d shows that the equivalent stress curve presents the decrease at first and then the stabilization in cases of node 1′ and node 2′. Equivalent stress curves at nodes 3′, 4′ and 5′ slightly away from the contact surface maintain the stabilization. The maximum equivalent stress of brake shoe is inside the brake shoe.

The equivalent stress reaches the maximum value at node 3′ at the initial state of emergency braking as compared to the later stage in the case of node 4′.

3.2.3. Contact Pressure Distribution

Figure 10 shows distributions of contact pressure at contact surfaces of brake disc and brake shoe at the start, at 0.07 s, at 3.38 s and at the end of emergency braking. Along the radial direction of brake shoe surface, the contact pressure reaches the maximum value at the average friction radius and decreases towards both sides. Along the circumferential direction, the contact pressure reaches the maximum value at the inlet of brake shoe and gradually decreases from the inlet to the outlet attributed to the edge effect. The contact pressure of the node reaches the maximum value at the average friction radius of the inlet location of brake shoe, which causes thermal cracks and thereby greatly affects braking properties between brake disc and brake shoe.

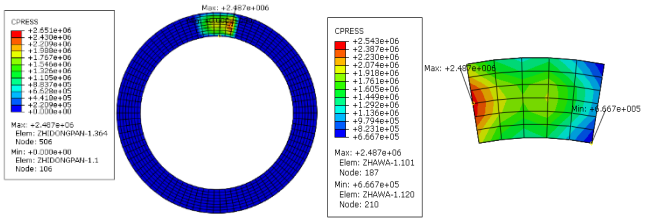

(**a**) At the start

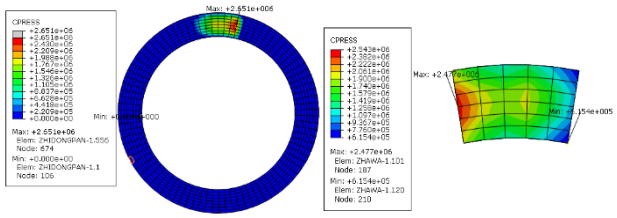

(**b**) t = 0.07 s

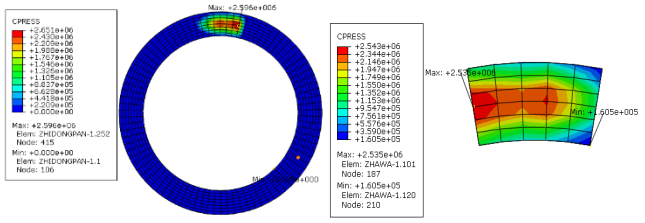

(**c**) t = 3.38 s

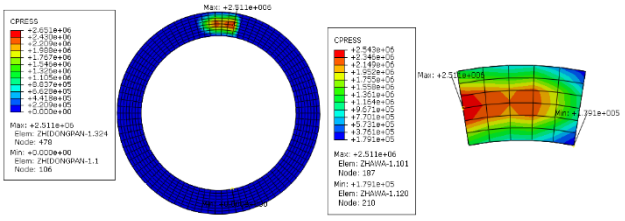

(**d**) At the end

Figure 10. Contact pressure distributions of contact surfaces of brake disc and brake shoe during emergency braking.

3.3. Validation of Finite Element Model Based on the Engineering Failure Case

In the multi-rope friction hoist of a coal mine in northeastern China, the accident of the high-speed reversal of a skip occurred suddenly at the end of lifting. Although the emergency braking is applied, the skip crashes towards the bottom of wellbore with the maximum reversal speed exceeding 20 m/s.

Figure 11 shows lots of discontinuous burn marks at the brake disc surface and crack marks at the brake shoe surface. Burn marks near the average friction radii of brake disc and brake shoe are attributed to the high temperature and high stress at contact surfaces during emergency braking with a high speed exceeding 20 m/s, which coincides well with temperature and stress distribution results in Section 3. Discontinuous marks of brake disc may be induced by the frictional chatter characteristics between brake disc and brake shoe. Therefore, the frictional flutter characteristics between brake disc and brake shoe should be investigated.

Figure 11. Surface damages of brake disc and brake shoe after emergency braking of coal mine hoist with high speed and heavy load.

4. Frictional Flutter Characteristics between Brake Disc and Brake Shoe

During braking between brake disc and brake shoe, the disk brake exhibits the self-excited vibration, which causes frictional flutter characteristics between brake disc and brake shoe and thereby induces braking failure attributed to insufficient brake torque. Therefore, it is of great importance to explore frictional flutter characteristics between brake disc and brake shoe to ensure the braking safety and reliability.

4.1. Theoretical Background

Based on the geometric model of a disc brake shoe in Section 2, the simplified principle diagram of self-excited vibration of disc brake is established as shown in Figure 12a and thereby double degrees of freedom vibration mechanism model is established as shown in Figure 12b. In the model, spring and damping elements are employed to restrict motions of brake disc and brake shoe along the X direction. The normal braking load acts on the brake shoe to apply the braking force between brake shoe and brake disc. The dynamic equation of the disc brake system is given by Equation (11) [20], which can be described as Equations (12) and (13) using the stated equations.

$$\begin{cases} m_1\ddot{x}_1 + c_{1x}\dot{x}_1 + k_{1x}x_1 = F_{fx}(v_0 + \dot{x}_2 - \dot{x}_1) \\ m_2\ddot{x}_2 + c_{2x}\dot{x}_2 + k_{2x}x_2 = -F_{fx}(v_0 + \dot{x}_2 - \dot{x}_1) \end{cases} \tag{11}$$

$$\begin{cases} X_1 = x_1 \\ V_1 = \dot{x}_1 \\ X_2 = x_2 \\ V_2 = \dot{x}_2 \end{cases} \tag{12}$$

$$\begin{cases} \dot{X}_1 = V_1 \\ \dot{V}_1 = \frac{1}{m_1}(F_{fx}(v_r) - c_1V_1 - k_1X_1) \\ X_2 = V_2 \\ \dot{V}_2 = \frac{1}{m_2}(-F_{fx}(v_r) - c_2V_2 - k_2X_2) \end{cases} \tag{13}$$

where m_1 and m_2 represent the mass of brake shoe and brake disc, respectively, k_{1x} and c_{1x} denote the stiffness and damping of brake shoe, respectively, k_{2x} and c_{2x} are the stiffness and damping of brake disc, respectively, and F_{fx} is the friction force.

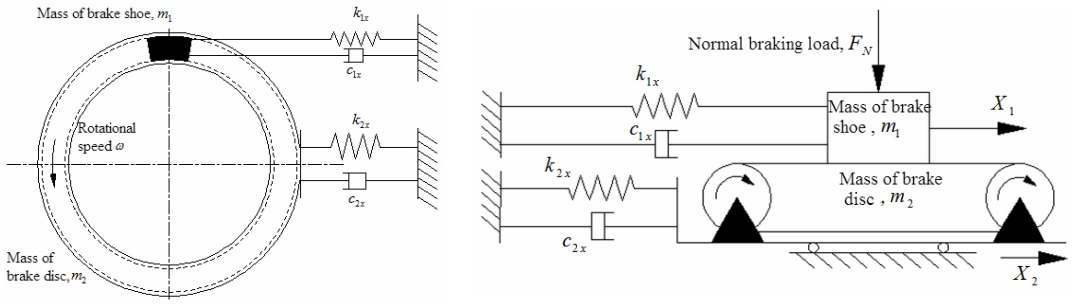

(**a**) (**b**)

Figure 12. The dynamic model of the disc brake shoe. (**a**) Simplified dynamic model of brake shoe and brake disc. (**b**) Dynamics model of disc brake system.

According to the Stribeck friction model (Figure 13), the friction force between brake disc and brake shoe F_{fx} is described as Equation (14). In the equation, the dynamic coefficient of friction $\mu(v_r)$ is given by Equation (15). The relative sliding velocity is written as $v_r = v_0 + \dot{x}_2 - \dot{x}_1$. δ, γ and η are three correction coefficients in the equation; usually, δ ranges from 0 to 1, γ and η are positive values. According to the studies on vibration and noise of stick-slip motion by Popp and Stelter [20,21], δ, γ and η are equal to 0.05, 0.03 and 0.0000134637, respectively. Based on Equations (11)–(15), frictional flutter characteristics between brake disc and brake shoe can be analyzed using Matlab simulation.

$$F_{fx}(v_r) = \mu(v_r)|F_N|\mathrm{sgn}(v_r) \tag{14}$$

$$\mu(v_r) = \begin{cases} \frac{1-\delta}{1-\gamma} + \delta + \eta^2 & v_r > 0 \\ \frac{1-\delta}{1-\gamma} - \delta - \eta^2 & v_r < 0 \end{cases} \tag{15}$$

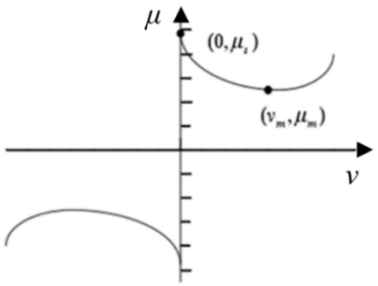

Figure 13. The nonlinear Stribeck friction model.

4.2. Effects of Braking Parameters on the Flutter Characteristics between Brake Disc and Brake Shoe

(1) Effect of initial braking speed

The simulation parameters are: $k_1 = 1$ N/m, $k_2 = 1$ N/m, $c_1 = 0.1$ N·s/m, $c_2 = 0.1$ N·s/m, $m_1 = 0.035$ kg, $m_2 = 2.959$ kg and $N = 10$ N [12]. In order to explore the effect of initial braking speed on flutter characteristics between brake disc and brake shoe, initial braking speeds, v_0, are equal to 10 m/s and 20 m/s according to Section 2. Figure 14a and c present the flutter phenomenon between the brake disc and brake shoe. At the initial stage of emergency braking, both contacting components show large vibration amplitudes. As the brake time increases, the vibration amplitude decreases gradually. Figure 14b shows small radii and number of instability limit cycles in the speed-displacement diagram of the brake shoe, which indicates the small vibration amplitude and a short period to reach stabilization. However, in the speed-displacement diagram of the brake disc (Figure 14d), larger radii and number of instability limit cycles reveal larger vibration amplitudes and a longer period is needed to reach

stabilization. It is obviously observed from Figure 15 that as the initial braking speed increases from 10 to 20 m/s, vibration amplitudes of both the brake disc and brake shoe decrease as well as the radii and number of instability limit cycles in the speed-displacement diagrams, which indicates a decrease in the period required to reach stabilization. At the initial braking speed of 20 m/s, an increase in braking time induces the vibration amplitude to decrease to zero.

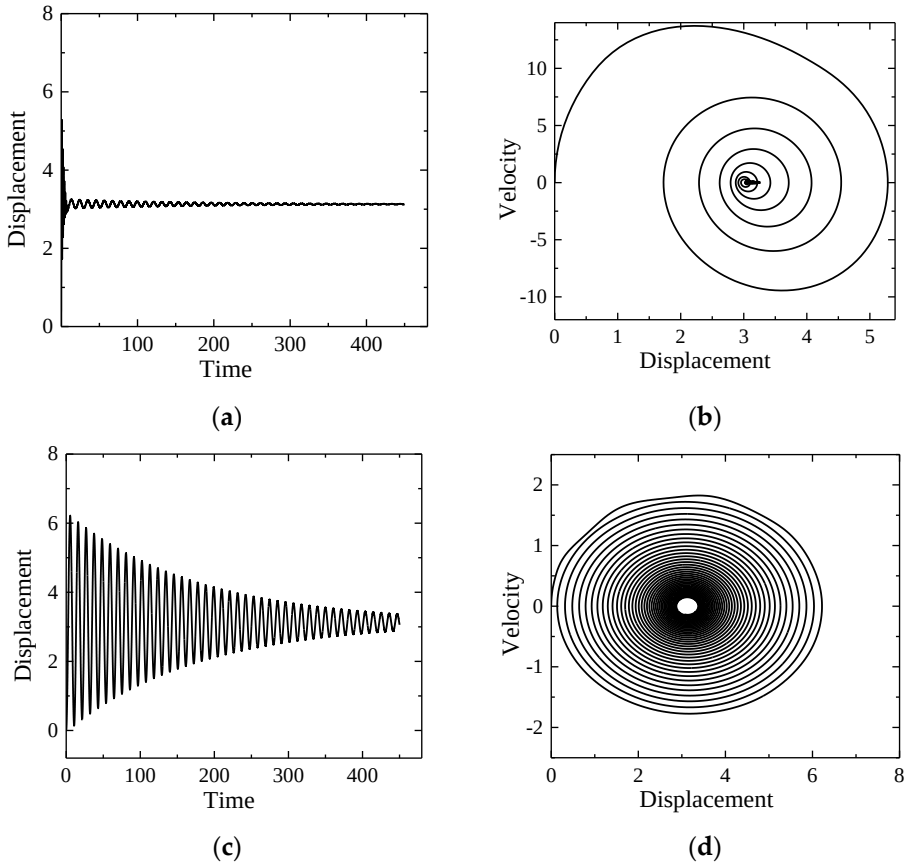

Figure 14. Evolutions of the displacement and speed-displacement diagram of brake disc and brake shoe at the initial braking speed of 10 m/s. (**a**) Evolution of the displacement of the brake shoe. (**b**) Evolution of the speed-displacement diagram of the brake shoe. (**c**) Evolution of the displacement of the brake disc. (**d**) Evolution of the speed-displacement diagram of the brake disc.

(2) Effect of normal braking load

The simulation parameters are: k_1 = 1 N/m, k_2 = 1 N/m, c_1 = 0.1 N·s/m, c_2 = 0.1 N·s/m, m_1 = 0.035 kg, m_2 = 2.959 kg and v_0 = 20 m/s. In order to explore the effect of normal braking load on flutter characteristics between brake disc and brake shoe, the normal braking loads are 80 N, 120 N and 180 N according to Section 2. Evolutions of displacement versus time of brake disc and brake shoe in Figures 16–18 show that at a small normal braking load, the vibration amplitude of the brake disc increases gradually until the vibration state with a stable constant amplitude; the brake shoe presents a small displacement amplitude. An increase in normal braking load induces the vibration with a constant amplitude and an increase in the vibration amplitude in cases of a brake disc and brake shoe. Figure 16b,d show that the brake disc and brake shoe both show the long period from instability to stability limit cycles during emergency braking. At the initial stage of emergency braking, the relative sliding between brake disc and brake shoe corresponds to small instability limit cycle. At the later stage, the stick-slip state between brake disc and brake shoe corresponds to larger stability limit cycles. As the normal braking load increases, the period from instability to stability limit cycles shortens in cases of speed-displacement diagrams, which indicates the quick entrance to the stage of

vibration with stable amplitude in the case of both the brake disc and brake shoe. According to the speed-displacement diagram, the disc brake presents the irregular ellipse of the limit cycle at each normal braking load as compared to the scallop of the brake shoe.

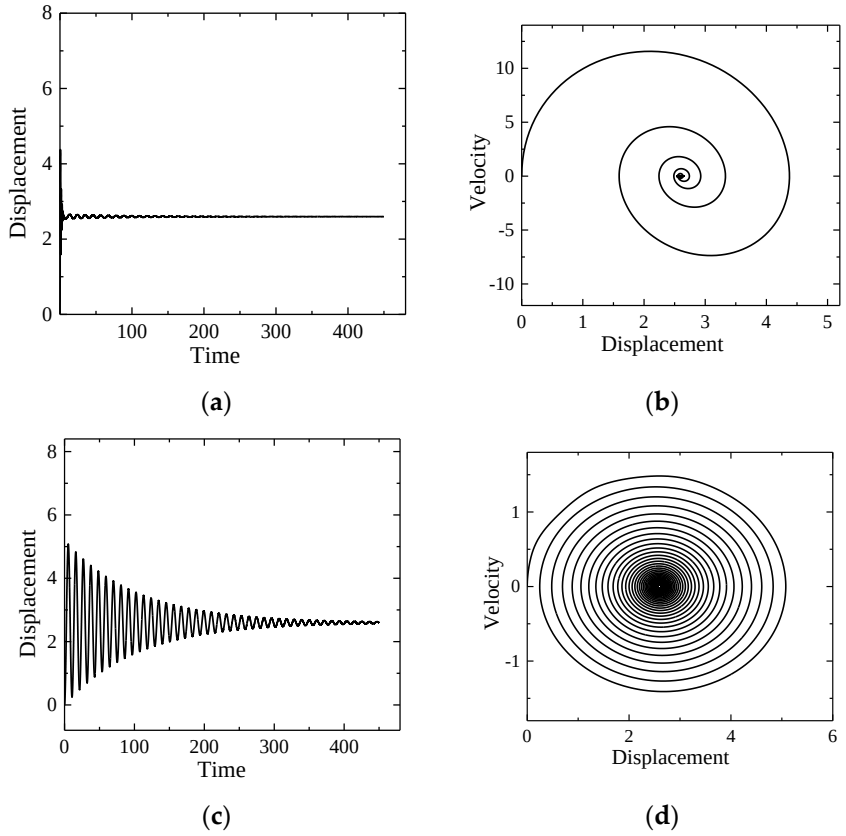

Figure 15. Evolutions of the displacement and speed-displacement diagram of brake disc and brake shoe at the initial braking speed of 20 m/s. (**a**) Evolution of the displacement of the brake shoe. (**b**) Evolution of the speed-displacement diagram of the brake shoe. (**c**) Evolution of the displacement of the brake disc. (**d**) Evolution of the speed-displacement diagram of the brake disc.

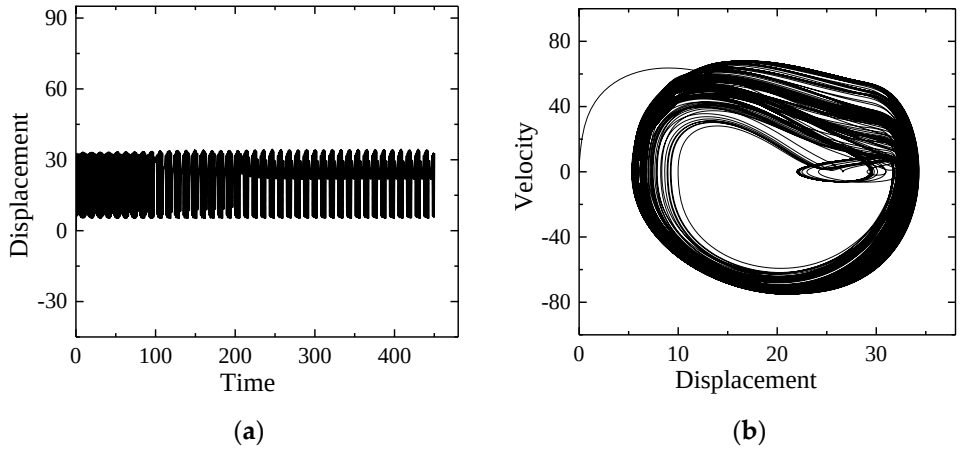

Figure 16. *Cont.*

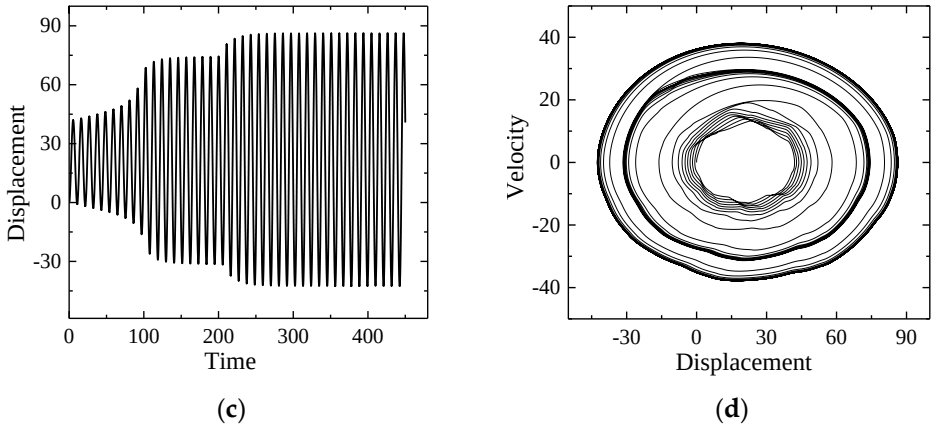

Figure 16. Evolutions of the displacement and speed-displacement diagram of brake disc and brake shoe at the normal braking load of 80 N. (**a**) Evolution of the displacement of the brake shoe. (**b**) Evolution of the speed-displacement diagram of the brake shoe. (**c**) Evolution of the displacement of the brake disc. (**d**) Evolution of the speed-displacement diagram of the brake disc.

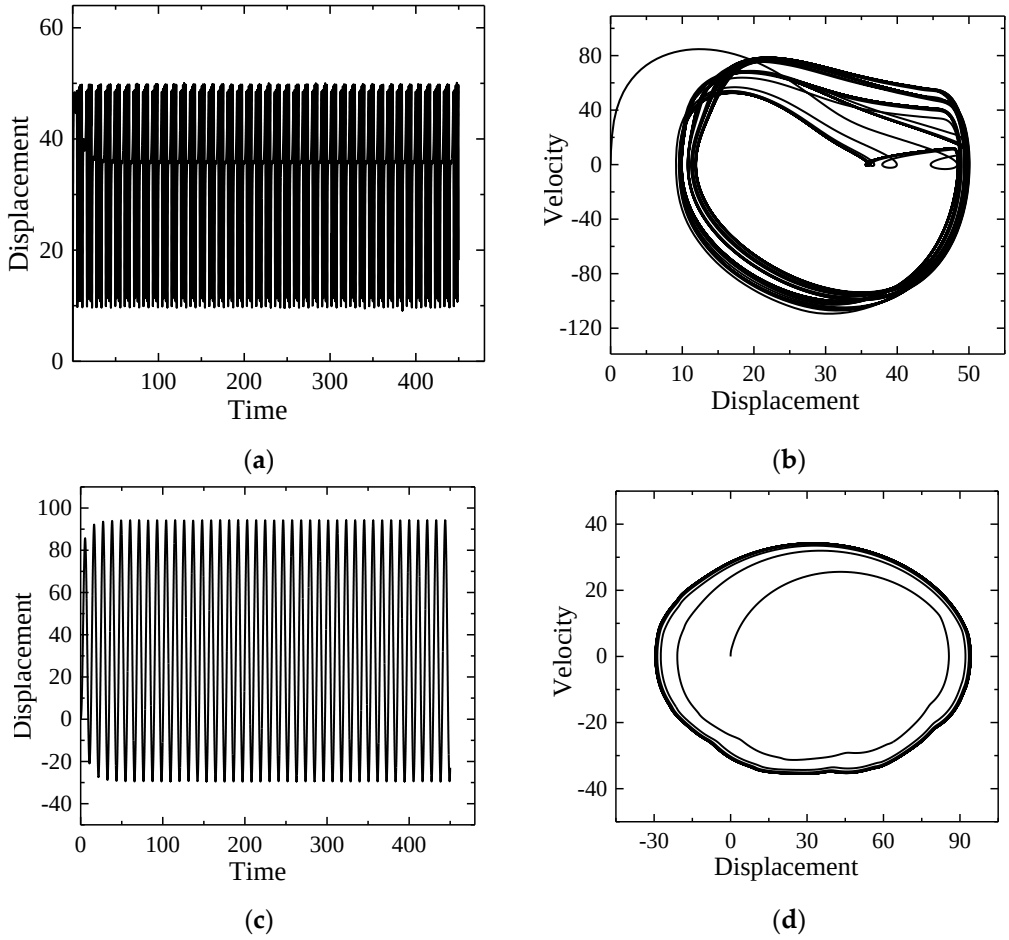

Figure 17. Evolutions of the displacement and speed-displacement diagram of brake disc and brake shoe at the normal braking load of 120 N. (**a**) Evolution of the displacement of the brake shoe. (**b**) Evolution of the speed-displacement diagram of the brake shoe. (**c**) Evolution of the displacement of the brake disc. (**d**) Evolution of the speed-displacement diagram of the brake disc.

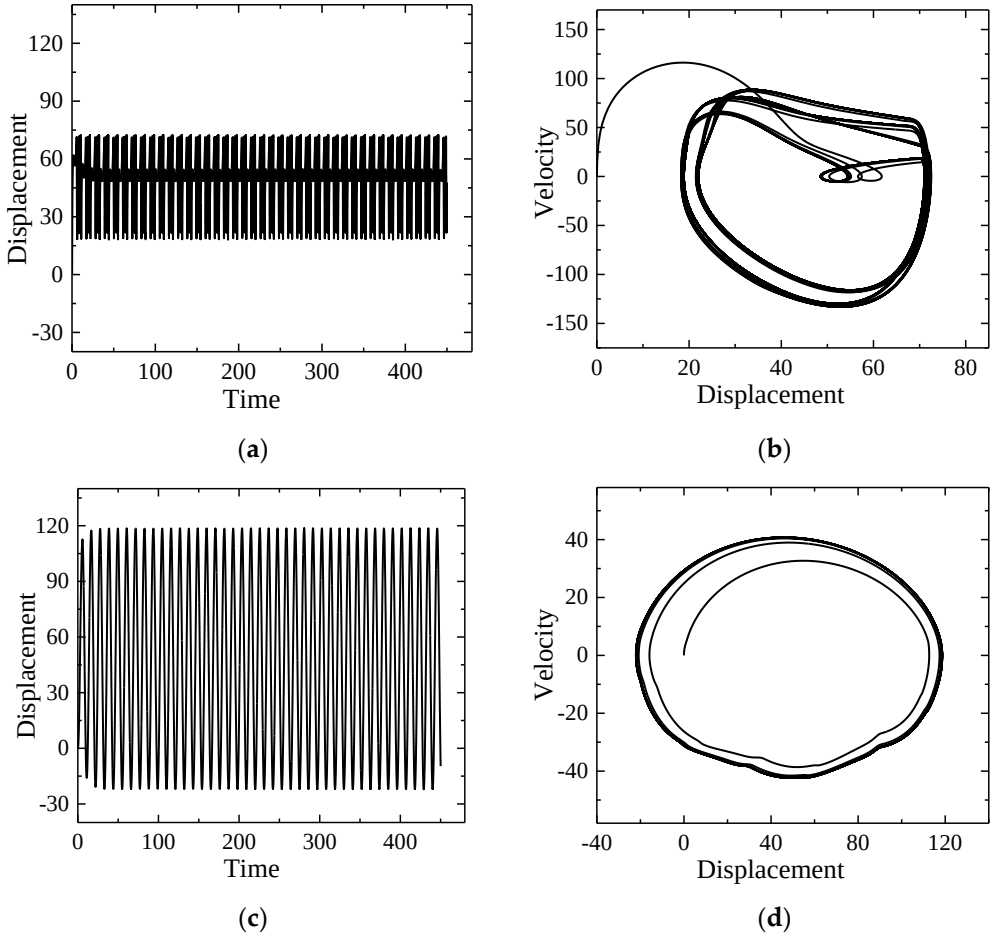

Figure 18. Evolutions of the displacement and speed-displacement diagram of brake disc and brake shoe at the braking load of 180 N. (**a**) Evolution of the displacement of the brake shoe. (**b**) Evolution of the speed-displacement diagram of the brake shoe. (**c**) Evolution of the displacement of the brake disc. (**d**) Evolution of the speed-displacement diagram of the brake disc.

(3) Effect of damping parameter

The simulation parameters are: k_1 = 1 N/m, k_2 = 1 N/m, m_1 = 0.035 kg, m_2 = 2.959 kg, v_0 = 20 m/s and N = 10 N. In order to explore the effect of damping parameter on flutter characteristics between brake disc and brake shoe, damping parameters are c_1 = 0.1 N·s/m, c_2 = 0.1 N·s/m and c_1 = 0.1 N·s/m, c_2 = 0.4 N·s/m. Figure 19a,c show that the vibration amplitude of brake disc decreases gradually. The vibration amplitude of brake shoe decreases rapidly and then sustains stabilization. The brake disc presents a longer time reaching stabilization as compared to the brake shoe. Figure 19b,d show lots of instability limit cycles in the speed-displacement diagram of the disc brake and no stability limit point, which indicates the continuous vibration of the disc brake. In the case of the brake shoe, there are fewer instability limit cycles and finally the stability limit point forms, which reveals the small vibration amplitude of brake shoe. As the damping parameter increases (Figures 19 and 20), the instability limit cycles gradually approach the center and form the stability limit point in the speed-displacement diagram of disc brake. The vibration amplitude decreases and presents a shorter time to reach the stability limit point in cases of the brake disc and brake shoe.

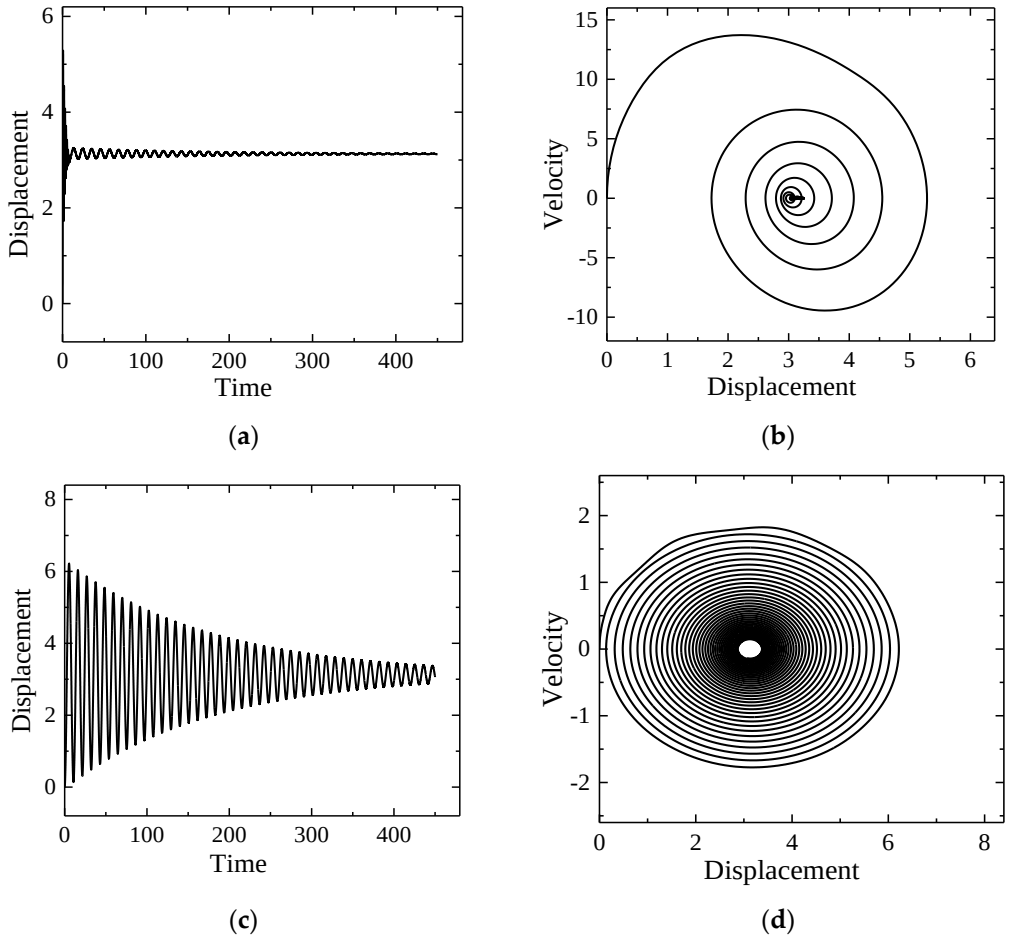

Figure 19. Evolutions of the displacement and speed-displacement diagram of brake disc and brake shoe at the damping of $c_1 = c_2 = 0.1$ N·s/m. (**a**) Evolution of the displacement of the brake shoe. (**b**) Evolution of the speed-displacement diagram of the brake shoe. (**c**) Evolution of the displacement of the brake disc. (**d**) Evolution of the speed-displacement diagram of the brake disc.

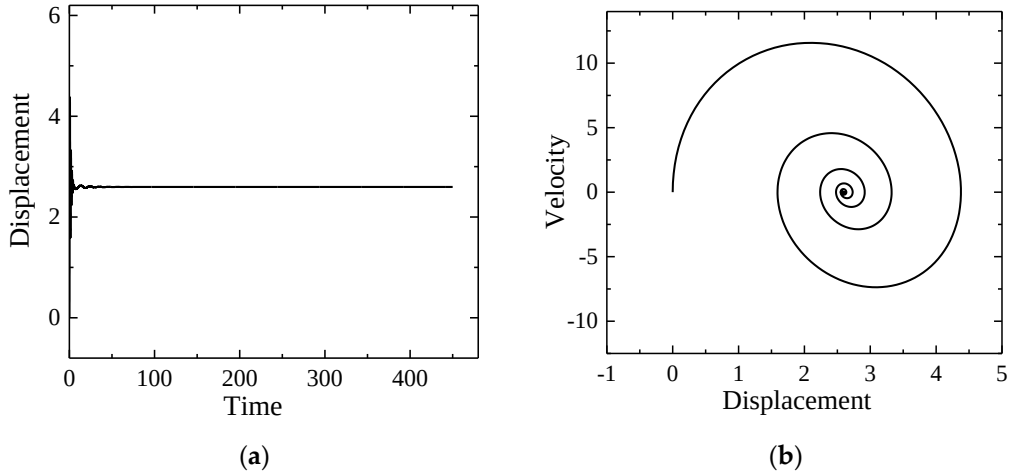

Figure 20. *Cont.*

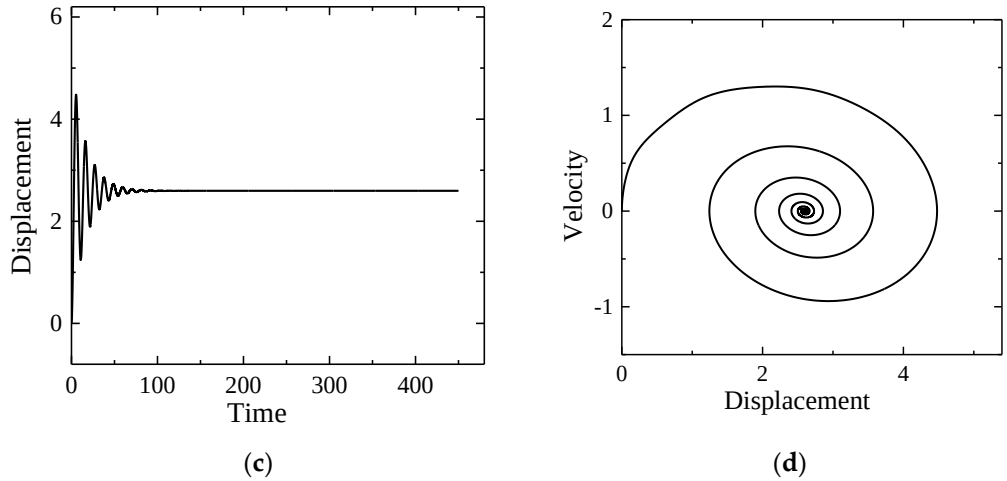

Figure 20. Evolutions of the displacement and speed-displacement diagram of brake disc and brake shoe at the damping of c1 = 0.1 N·s/m and c2 = 0.4 N·s/m. (**a**) Evolution of the displacement of the brake shoe. (**b**) Evolution of the speed-displacement diagram of the brake shoe. (**c**) Evolution of the displacement of the brake disc. (**d**) Evolution of the speed-displacement diagram of the brake disc.

(4) Effect of stiffness parameter

The simulation parameters are: m_1 = 0.035 kg, m_2 = 2.959 kg, c_1 = 0.1 N·s/m, c_2 = 0.1 N·s/m, v_0 = 20 m/s and N = 10 N. In order to explore the effect of stiffness parameter on flutter characteristics between brake disc and brake shoe, the stiffness parameters are k_1 = 0.5 N/m, k_2 = 1 N/m and k_1 = 1 N/m, k_2 = 5 N/m. Figure 21 shows large variation amplitudes of brake disc and brake shoe. An increase in time induces the decrease in the vibration amplitude and then stabilization in both cases. The speed-displacement diagram presents lots of instability limit cycles and then stabilizes for the disc brake. In the case of the brake shoe, the speed-displacement diagram shows several instability limit cycles with a large radius at the start; the vibration amplitude decreases and finally stabilizes to the stability limit point. It is clearly seen from Figures 21 and 22 that an increase in stiffness induces decreases in the vibration amplitude and time reaching stabilization, and increases in the vibration frequency and number of instability limit cycles.

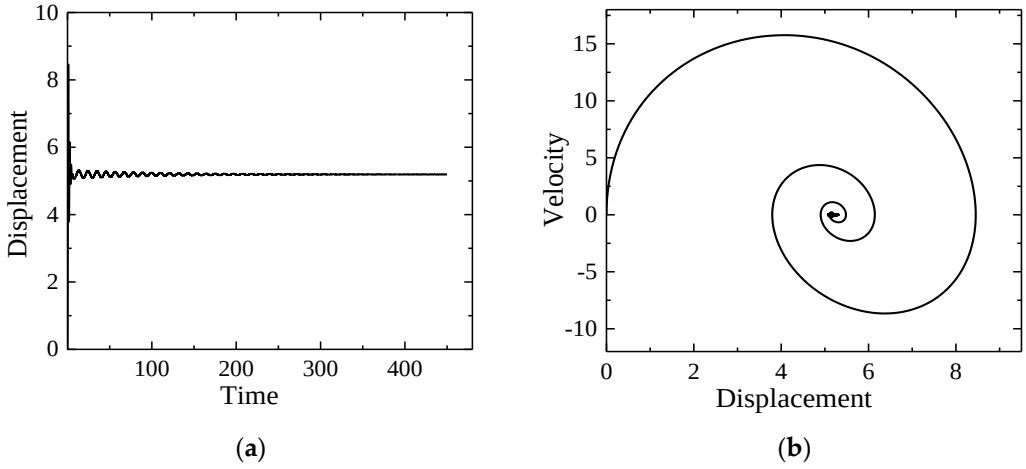

Figure 21. *Cont.*

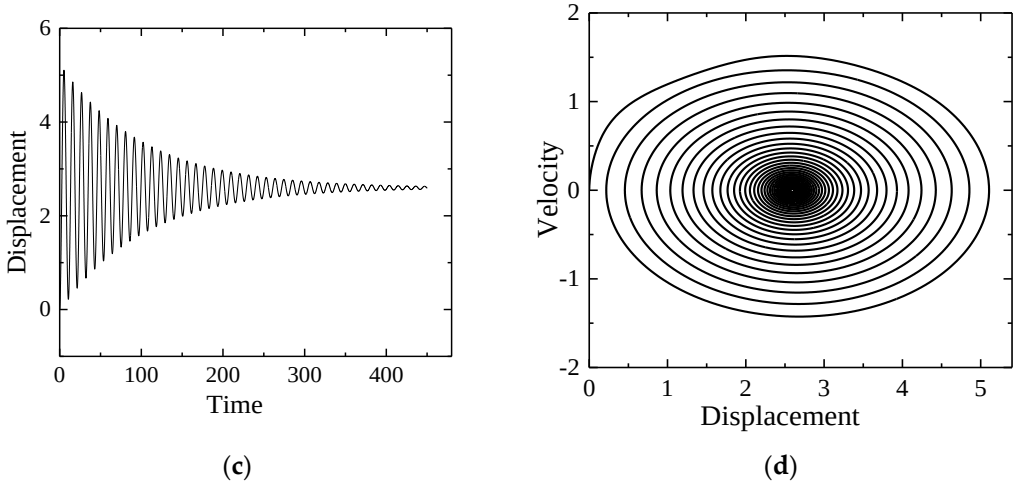

Figure 21. Evolutions of the displacement and speed-displacement diagram of brake disc and brake shoe at the stiffness of k_1 = 0.5 N/m and k_2 = 1 N/m. (**a**) Evolution of the displacement of the brake shoe. (**b**) Evolution of the speed-displacement diagram of the brake shoe. (**c**) Evolution of the displacement of the brake disc. (**d**) Evolution of the speed-displacement diagram of the brake disc.

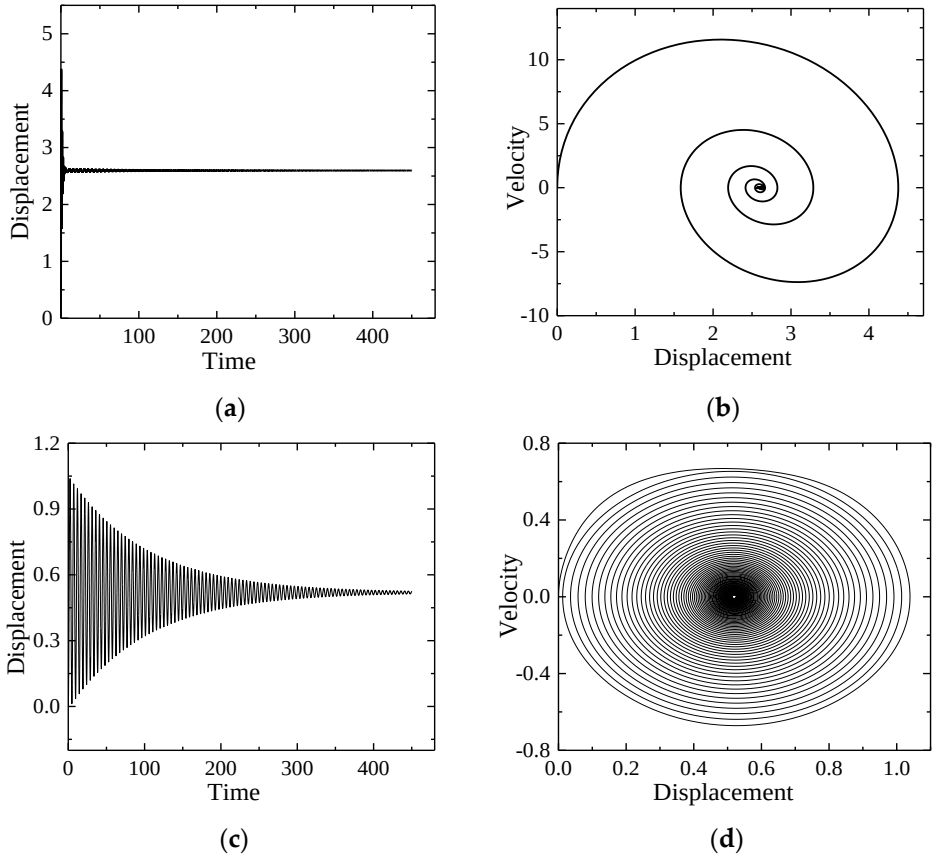

Figure 22. Evolutions of the displacement and speed-displacement diagram of brake disc and brake shoe at the stiffness of k_1 = 1 N/m and k_2 = 5 N/m. (**a**) Evolution of the displacement of the brake shoe. (**b**) Evolution of the speed-displacement diagram of the brake shoe. (**c**) Evolution of the displacement of the brake disc. (**d**) Evolution of the speed-displacement diagram of the brake disc.

5. Conclusions

The thermo-mechanical finite element model is established to investigate coupled thermo-mechanical behaviors of the brake disc and brake shoe of a deep coal mine hoist at a

high speed and with a large specific pressure. The temperature field of the brake shoe surface decreases from the outlet to the inlet, while the temperature field of the brake disc decreases along the rotational direction. The equivalent Von Mises stress decreases from the inlet to the outlet of brake shoe surface. The location at the average friction radius is less affected by the heat conduction and convective heat transfer in case of brake disc and brake shoe. The maximum temperature, the equivalent Von Mises stress and the contact pressure are all located at the average friction radii of brake disc and brake shoe surfaces during emergency braking. The engineering failure case of a skip crashing accident of a coal mine hoist at high speed and with a heavy load indicates crack marks on the brake shoe surface and discontinuous burn marks on the brake disc surface, which validates the finite element model and reveals the research importance of frictional chatter characteristics between the brake disc and the brake shoe. The time duration of friction flutter behavior decreases with increasing initial braking speed and damping factor, the flutter amplitude of the disc brake increases with increasing braking pressure, and the flutter frequency of the disc brake increases with increasing stiffness.

Author Contributions: Conceptualization, D.W.; methodology, D.W., R.W. and T.H.; validation, D.W., R.W. and T.H.; formal analysis, D.W., R.W. and T.H.; investigation, R.W. and T.H.; data curation, R.W. and T.H.; writing—original draft preparation, R.W. and T.H.; writing—review and editing, D.W.; visualization, G.X. and D.Z.; supervision, D.W.; project administration, G.X.; funding acquisition, D.W. All authors have read and agreed to the published version of the manuscript.

Funding: The research was supported by the National Key Research and Development Program (2016YFC0600907).

Acknowledgments: The authors wish to thank Top-Notch Academic Programs Project of Jiangsu Higher Education Institutions (TAPP) and a project funded by the Priority Academic Program Development of Jiangsu Higher Education Institutions (PAPD).

Conflicts of Interest: The authors declare no conflict of interest.

References

1. Wang, D.G.; Wang, R.X.; Zhang, J. Dynamic brake characteristics of disc brake during emergency braking of the kilometer deep coal mine hoist. *Adv. Mech. Eng.* **2020**, *12*, 1–23. [CrossRef]
2. Zhu, Z.C.; Peng, Y.X.; Shi, Z.Y.; Chen, G.A. Three-dimensional transient temperature field of brake shoe during hoist's emergency braking. *Appl. Therm. Eng.* **2009**, *29*, 932–937. [CrossRef]
3. Peng, Y.X.; Zhu, Z.C.; Chen, G.A.; Bao, J.S.; Liu, B.B.; Li, Y.L. Temperature field of disc brake for mine hoist. *J. Comput. Theor. Nanos* **2011**, *4*, 2380–2384. [CrossRef]
4. Bao, J.S.; Zhu, Z.C.; Tong, M.M.; Yin, Y.; Peng, Y.X. Influence of braking pressure on tribological performance of non-asbestos brake shoe for mine hoister during emergency braking. *Ind. Lubr. Tribol.* **2013**, *64*, 230–236. [CrossRef]
5. Yevtushenko, A.A.; Matysiak, S.J.; Ivanyk, E.G. Influence of periodically layered material structure on the frictional temperature during braking. *Int. J. Heat Mass Transf.* **1997**, *40*, 2115–2122. [CrossRef]
6. Yevtushenko, A.A.; Grzes, P. Mutual influence of the sliding velocity and temperature in frictional heating of the thermally nonlinear disc brake. *Int. J. Therm. Sci.* **2016**, *102*, 254–262. [CrossRef]
7. Zhou, K.; Dong, M.S.; Song, L.; Wang, J.Q. Simulation Analysis and Structure Optimization of Mine Brake Disc. *Int. Core J. Eng.* **2017**, *3*, 102–106.
8. Choi, J.H.; Lee, I. Finite element analysis of transient thermoelastic behaviors in disk brakes. *Wear* **2004**, *257*, 47–58. [CrossRef]
9. Wang, D.C. Research on Characteristics of Thermo-Mechanical Coupling and Prediction on Fatigue Life of Disc Brake. Master's Thesis, Shanghai University of Engineering Science, Shanghai, China, 2015.
10. Zhang, L.J.; Chen, Y.; Diao, K.; Meng, D.J. Computational investigation into disc-pads pressure distribution and thermomechanical coupling characteristics of brake pads in disc brake. *J. Tongji Univ. Nat. Sci. Ed.* **2013**, *41*, 1554–1561.
11. Xu, D.B. The FEA and Experimental Study on Emergency Braking of Brake Disc Based on the Theory of Thermo-Mechanical Coupling. Master's Thesis, Southwest Jiaotong University, Chengdu, China, 2017.
12. Li, Y.Y.; Ding, W.C.; Li, F.; Zhang, H. Calculation and analysis of critical chattering velocity in brake system. *Lubr. Eng.* **2011**, *36*, 49–52.

13. Eriksson, M.; Jacobson, S. Friction behaviour and squeal generation of disc brakes at low speeds. *Proc. Inst. Mech. Eng.* **2001**, *215*, 1245–1256. [CrossRef]
14. Manish, P.; Mahajanb, A.; Jarlen, D.; Chu, T.P.; Filip, P. Noise and vibration analysis of a disc-brake system using a stick-slip friction model involving coupling stiffness. *J. Sound Vib.* **2005**, *282*, 1273–1284.
15. Huang, Q.J. Research and Development of Friction Brake Squeal Noise Scaling Test Rig for High Speed Train. Master's Thesis, Southwest Jiaotong University, Chengdu, China, 2015.
16. Zhao, X.L. Study on the Principle and Test Method of the Scaling Test of the Friction Material and Its Equipment. Ph.D. Thesis, Jilin University, Changchun, China, 2007.
17. Liu, F.F. The Thermo-Mechanical Coupling Behavior of Brake Shoe during Emergency Braking of Hoist. Master's Thesis, China University of Mining and Technology, Xuzhou, China, 2011.
18. Zhao, Y.J. Simulation and Analysis of Disc Brake Coupled Thermal-Stress Transient Temperature. Master's Thesis, Huazhong University of Science and Technology, Wuhan, China, 2013.
19. Lu, D. Modeling and analysis of thermal flow multi-field coupled in disc brake based on ABAQUS. *Mach. Des. Manuf.* **2017**, *8*, 197–201.
20. Qiu, M.; Qian, Y.M. *Principal and Design of Tribology*; National Defense Industry Press: Beijing, China, 2013.
21. Popp, K.; Stelter, P. Stick-slip virbrations and chaos. *Philos. Trans. Phys. Sci. Eng.* **1990**, *332*, 89–105.